Tjark Heitmann*, Jonas Richter, Dennis Schubert and Robin Steinigeweg*

Selected applications of typicality to real-time dynamics of quantum many-body systems

https://doi.org/10.1515/ZNA-2020-0010
Received January 9, 2020; accepted March 11, 2020

Abstract: Loosely speaking, the concept of quantum typicality refers to the fact that a single pure state can imitate the full statistical ensemble. This fact has given rise to a rather simple but remarkably useful numerical approach to simulate the dynamics of quantum many-body systems, called *dynamical quantum typicality* (DQT). In this paper, we give a brief overview of selected applications of DQT, where particular emphasis is given to questions on transport and thermalization in low-dimensional lattice systems like chains or ladders of interacting spins or fermions. For these systems, we discuss that DQT provides an efficient means to obtain time-dependent equilibrium correlation functions for comparatively large Hilbert-space dimensions and long time scales, allowing the quantitative extraction of transport coefficients within the framework of, e. g., linear response theory (LRT). Furthermore, it is discussed that DQT can also be used to study the far-from-equilibrium dynamics resulting from sudden quench scenarios, where the initial state is a thermal Gibbs state of the pre-quench Hamiltonian. Eventually, we summarize a few combinations of DQT with other approaches such as numerical linked cluster expansions or projection operator techniques. In this way, we demonstrate the versatility of DQT.

Keywords: low-dimensional lattice models; numerical simulation; quantum many-body dynamics; quantum typicality; transport and thermalization.

***Corresponding authors: Tjark Heitmann**, Department of Physics, University of Osnabrück, Osnabrück, D-49069, Germany, E-mail: tjark.heitmann@uos.de, https://orcid.org/0000-0001-7728-0133, and; **Robin Steinigeweg**, Department of Physics, University of Osnabrück, Osnabrück, D-49069, Germany, E-mail: rsteinig@uos.de, https://orcid.org/0000-0003-0608-0884.
Jonas Richter and Dennis Schubert: Department of Physics, University of Osnabrück, Osnabrück, D-49069, Germany. https://orcid.org/0000-0003-2184-5275 (J. Richter)

Published online April 27, 2020

1 Introduction

Unraveling the dynamics of isolated quantum many-body systems is a central objective of modern experimental and theoretical physics. On the one hand, new experimental platforms composed of cold atoms or trapped ions have opened the door to perform quantum simulations with a high amount of control over Hamiltonian parameters and initial conditions [1, 2]. On the other hand, there has been substantial progress from the theoretical side to understand (i) experimental observations and (ii) long-standing questions about the fundamentals of statistical mechanics [3–7]. One such question is how to reconcile the emergence of thermodynamic behavior with the unitary time evolution of isolated quantum systems, i. e., to explain whether and in which way an isolated system relaxes towards a stationary long-time state which agrees with the predictions from standard statistical mechanics. Another similarly intriguing question in this context is to explain the onset of conventional hydrodynamic transport, i. e., diffusion, from truly microscopic principles [8–10]. The numerical analysis of thermalization and transport in isolated quantum many-body systems is at the heart of this paper.

Generally, the theoretical analysis of quantum many-body dynamics is notoriously difficult. Given a quantum system $\mathcal{H}$ and an arbitrary nonequilibrium state $\rho(0)$, universal concepts to describe the resulting dynamics are rare [11–13], and one is usually required to solve the microscopic equation of motion for the density matrix $\rho(t)$, i. e., the von-Neumann equation

$$\frac{d}{dt}\rho(t) = -i[\mathcal{H}, \rho(t)] \tag{1}$$

($\hbar = 1$) which, in the case of a pure state $\rho(t) = |\psi(t)\rangle\langle\psi(t)|$, reduces to the Schrödinger equation

$$\frac{d}{dt}|\psi(t)\rangle = -i\mathcal{H}|\psi(t)\rangle\,. \tag{2}$$

While the presence of strong interactions often prohibits any analytical solution, numerical studies of Eq. (2) are plagued by the exponential growth of the Hilbert space upon increasing the number of degrees of freedom. Moreover, since thermalization and transport can potentially be

very slow processes, the necessity to study long time scales adds another layer of complexity.

Of course, for situations close to equilibrium, e. g., a system being weakly perturbed by an external force, linear response theory (LRT) provides a successful framework to describe the system's response in terms of dynamical correlation functions evaluated exactly at equilibrium [14]. However, analogous to Eqs. (1) and (2), the calculation of such time-dependent correlation functions for large system sizes and long time scales is a severe challenge in practice.

Despite these difficulties, significant progress has been made over the years thanks to the augmented availability of computational resources and the development of sophisticated numerical techniques. Especially for one-dimensional systems the time-dependent density matrix renormalization group (tDMRG), including related methods based on matrix product states, provides a powerful approach to dynamical properties in the thermodynamic limit (for reviews, see [15, 16]). However, due to the inevitable build-up of entanglement, this approach is limited in the time scales which can be reached in simulations.

In the present paper, the focus is on another useful numerical approach to the dynamics of quantum many-body systems, which is based on the concept of dynamical quantum typicality (DQT) [17, 18]. In a nutshell, DQT means that "the vast majority of all pure states featuring a common expectation value of some generic observable at a given time will yield very similar expectation values of the same observable at any later time" [17]. In fact, the idea of using random vectors has a long and fruitful history [19–26]. By virtue of an iterative forward propagation of these vectors in real or imaginary time, dependencies on time and temperature can be obtained. Since DQT can be implemented rather memory efficiently, it is possible to study dynamical properties of quantum many-body systems with Hilbert-space dimensions significantly larger compared to standard exact diagonalization (ED). Moreover, there are no conceptual limitations on the reachable time scales.

It is worth pointing out that DQT can not only be used to obtain time-dependent properties [27–29] or spectral functions [22, 30–32] but also static properties such as the density of states [33] or thermodynamic quantities [34–37]. However, it is the aim of this paper to discuss the usefulness and versatility of DQT especially in the context of thermalization and transport.

This paper is structured as follows. In Sec. 2, we give a brief introduction to the concept of typicality and also elaborate on the differences between typicality and the eigenstate thermalization hypothesis (ETH). In Sec. 3, we discuss various applications of typicality to the dynamics of quantum many-body systems. Finally, we summarize and conclude in Sec. 4, where we also provide an outlook on further applications of DQT.

2 What is typicality?

Loosely speaking, the notion of typicality means that even a single pure quantum state can imitate the full statistical ensemble, or, more precisely, expectation values of typical pure states are close to the expectation value of the statistical ensemble [20, 23–26]. While typicality has been put forward as an important insight to explain the emergence of thermodynamic behavior (see e. g., Ref. [23] for an overview), let us here focus on the practical consequences of typicality. In particular, let us consider the, e. g., canonical equilibrium expectation value $\langle A\rangle_{\mathrm{eq}}$ of some (quasi-local) operator A defined as

$$\langle A\rangle_{\mathrm{eq}} = \frac{\mathrm{Tr}\left[Ae^{-\beta\mathcal{H}}\right]}{Z} = \frac{\mathrm{Tr}\left[e^{-\beta\mathcal{H}/2}Ae^{-\beta\mathcal{H}/2}\right]}{Z}, \tag{3}$$

where $Z = \mathrm{Tr}[\exp(-\beta\mathcal{H})]$ is the canonical partition function, $\beta = 1/T$ ($k_B = 1$) is the inverse temperature, and we have used the cyclic invariance of the trace. Exploiting typicality, it is possible to rewrite $\langle A\rangle_{\mathrm{eq}}$ according to

$$\langle A\rangle_{\mathrm{eq}} = \frac{\langle\psi_\beta \mid A \mid\psi_\beta\rangle}{\langle\psi_\beta \mid \psi_\beta\rangle} + \varepsilon, \tag{4}$$

where we have introduced the abbreviation $|\psi_\beta\rangle = e^{-\beta\mathcal{H}/2}|\psi\rangle$, which is sometimes referred to as thermal pure quantum state [36]. The reference pure state $|\psi\rangle$ is drawn at random from the full Hilbert space with finite dimension d according to the unitary invariant Haar measure [17], i. e.,

$$|\,\psi\,\rangle = \sum_{k=1}^{d} (a_k + ib_k)|k\rangle, \tag{5}$$

where the coefficients a_k and b_k are drawn from a Gaussian distribution with zero mean (other types of randomness have been suggested as well [19, 38]), and the pure states $|k\rangle$ denote orthogonal basis states of the Hilbert space. (Note that $|\psi\rangle$ is almost maximally entangled [39, 40].) Importantly, the standard deviation of the statistical error $\epsilon = \epsilon(|\psi\rangle)$ of the approximation (4) scales as $\sigma \propto 1/\sqrt{d_{\mathrm{eff}}}$, where $d_{\mathrm{eff}} = \mathrm{Tr}[\exp(-\beta(\mathcal{H} - E_0))]$ is the effective dimension

of the Hilbert space with E_0 being the ground-state energy of $\mathcal{H}$. Here we assume that A is a local operator (or a low-degree polynomial in system size), which applies to all examples discussed in this paper. For more details on error bounds see, e. g., Refs. [18, 36]. For empirical estimates, see, e. g., Ref. [41]. Thus, d_{eff} is essentially the number of thermally occupied states and, for $\beta = 0$, we have $d_{\text{eff}} = d$. As a consequence, increasing the number of degrees of freedom of a quantum many-body system, e. g., the number of lattice sites L, leads to an exponential improvement of the accuracy (the higher the temperature, the faster), and Eq. (4) becomes exact in the thermodynamic limit $L \to \infty$.

The typicality approximation (4) has proven to be very useful to calculate equilibrium quantities of quantum many-body systems such as the specific heat, entropy, or magnetic susceptibility [34–37, 41]. For the purpose of this review, however, it is most important to note that typicality is not just restricted to equilibrium properties, but also extends to the real-time dynamics of quantum expectation values [17, 27–29, 42–44]. This dynamical version of typicality forms the basis of the numerical approach to time-dependent correlation functions and out-of-equilibrium dynamics more generally, which is discussed in Sec. 3.

Let us briefly discuss the relationship between typicality and the ETH [45–47]. The ETH states that the expectation values of local observables evaluated within individual eigenstates $|n\rangle$ of generic (nonintegrable) Hamiltonians coincide with the microcanonical ensemble average at the corresponding energy density,

$$A_{nn} = \langle n|A|n\rangle = A_{\text{mc}}(E). \tag{6}$$

While this fact (i. e., pure states can approximate ensemble expectation values) appears similar to our discussion of typicality in the context of Eq. (4), let us stress that typicality and ETH are two distinct concepts. On the one hand, while the ETH is assumed to hold for few-body operators and nonintegrable models [5, 48–55], a rigorous proof for its validity is still absent. On the other hand, typicality is no assumption and essentially requires the largeness of the effective Hilbert-space dimension. This difference becomes particularly clear from the following point of view: since the distribution of the a_k and b_k in Eq. (5) is invariant under any unitary transformation, the state $|\psi\rangle$ is a random superposition also in the eigenbasis of $\mathcal{H}$ (whereas the ETH just refers to single eigenstates). Due to this randomness, Eq. (4) holds even in cases where the ETH breaks down, i. e., where the expectation values of observables exhibit strong eigenstate-to-eigenstate fluctuations.

Since typicality is independent of the validity of the ETH, it can be used in integrable or many-body localized models, where the ETH is expected to be violated [56–59]. As a side remark, typicality can also be used to test the ETH [60].

Eventually, let us emphasize that the choice of the specific basis $|k\rangle$ in Eq. (5) is arbitrary. Therefore, the random state $|\psi\rangle$ can be conveniently constructed in the working basis which is used to set up the Hamiltonian and all other observables. For instance, when working with spin-1/2 systems, a common choice is the so-called Ising basis, i. e., the states $|k\rangle$ then denote the 2^L different combinations of $\uparrow$ and $\downarrow$. Naturally, it is possible to combine DQT with the use of symmetries [61], where a random state is then drawn independently within each subsector.

3 DQT as a numerical tool

We now discuss the use of DQT as a numerical method. To begin with, we discuss in Sec. 3.1 the iterative forward propagation of pure states in large Hilbert spaces. Afterward, as a first application, we demonstrate in Sec. 3.2 how typicality can be used to study the (local) density of states. In Sec. 3.3, we then show how DQT can be used to evaluate equilibrium correlation functions within the framework of LRT. Sec. 3.4 is concerned with the out-of-equilibrium dynamics in certain quantum-quench scenarios. Eventually, in Sec. 3.5, we discuss how DQT can be combined with other approaches such as numerical linked cluster expansions or projection operator techniques.

3.1 Pure-state propagation

From a numerical point of view, a central advantage of the typicality approach comes from the fact that one can work with pure states instead of having to deal with full density matrices. This fact leads to a substantial reduction of the memory requirements, since it is possible to efficiently generate time and temperature dependencies of pure states. (Note that, while it is always possible to purify a density matrix, the DQT approach in contrast does not require to square the Hilbert-space dimension [62].)

Specifically, let us consider the pure state $|\psi_\beta\rangle = e^{-\beta\mathcal{H}/2}|\psi\rangle$ introduced in Eq. (4). The time evolution of $|\psi_\beta\rangle$ is given by $|\psi_\beta(t)\rangle = e^{-i\mathcal{H}t}|\psi_\beta\rangle$. The full evolution up to time t can be subdivided into a product of consecutive steps,

$$|\psi_\beta(t)\rangle = \left(e^{-i\mathcal{H}\delta t}\right)^N |\psi_\beta\rangle, \tag{7}$$

where $\delta t = t/N$ is a discrete time step. If δt is chosen sufficiently small, there is a variety of methods to accurately evaluate the action of the matrix exponential $e^{-i\mathcal{H}\delta t}$ without diagonalization of $\mathcal{H}$. A particularly simple approach in this context is a fourth-order Runge-Kutta (RK4) scheme, where the time evolution is approximated as [28, 29],

$$|\psi_\beta(t+\delta t)\rangle \approx |\psi_\beta(t)\rangle + \sum_{k=1}^{4} |f_k\rangle. \tag{8}$$

The four auxiliary states $|f_1\rangle - |f_4\rangle$ are constructed according to [28, 29],

$$|f_k\rangle = \frac{-i\mathcal{H}\delta t}{k}|f_{k-1}\rangle, \quad |f_0\rangle = |\psi_\beta(t)\rangle, \tag{9}$$

and the error of the approximation (8) scales as $\mathcal{O}(\delta t^5)$. Note that the RK4 scheme in Eqs. (8) and (9) is equivalent to a Taylor expansion of the exponential $e^{-i\mathcal{H}\delta t}$ up to fourth order. Note further that, in complete analogy to the propagation in real time, the temperature dependence of $|\psi_\beta\rangle$ can be generated by an evolution in small imaginary time steps $i\delta\beta$.

Apart from RK4, other common and more sophisticated methods to propagate pure states without diagonalization are, e. g., Trotter decompositions [34, 63], Krylov subspace techniques [64], as well as Chebyshev polynomial expansions [65–69]. A unifying property of all these methods and RK4 is the necessity to calculate matrix-vector products, i. e., to evaluate the action of the Hamiltonian $\mathcal{H}$ onto pure states. Importantly, such matrix-vector multiplications can be carried out relatively memory efficiently thanks to the sparse matrix structure of $\mathcal{H}$ in models with short-range interactions such as nearest-neighbor couplings. As a consequence, it is possible to numerically treat comparatively large system sizes, i. e., with huge Hilbert-space dimensions far beyond the range of ED.

3.2 Calculating the (local) density of states

As a first useful application, let us describe how pure states, in combination with a forward propagation in real time, can be used to evaluate the (local) density of states [33]. To begin with, we note that the density of states of some Hamiltonian $\mathcal{H}$ with eigenvalues E_n can be written as

$$\Omega(E) = \sum_n \delta(E - E_n) \tag{10}$$

$$= \frac{1}{2\pi}\int_{-\infty}^{\infty} e^{itE}\mathrm{Tr}\left[e^{-i\mathcal{H}t}\right]\mathrm{d}t, \tag{11}$$

where we have used the definition of the δ function. In the spirit of Eq. (4), we can approximate the trace in Eq. (11) by a scalar product with a randomly drawn pure state $|\psi\rangle$,

$$\mathrm{Tr}\left[e^{-i\mathcal{H}t}\right] \propto \langle\psi|e^{-i\mathcal{H}t}|\psi\rangle = \langle\psi \mid \psi(t)\rangle, \tag{12}$$

such that Eq. (11) can be approximated as

$$\Omega(E) \propto \int_{-t_{\max}}^{+t_{\max}} e^{itE}\langle\psi \mid \psi(t)\rangle\mathrm{d}t, \tag{13}$$

where $\langle\psi(0) \mid \psi(-t)\rangle = \langle\psi(0) \mid \psi(t)\rangle^*$, and $t_{\max}$ is the maximum time to which $|\psi(t)\rangle$ is evolved. Due to this cutoff time, the resulting energy resolution of $\Omega(E)$ is given by $\Delta E = \pi/t_{\max}$. Thus, the density of states of some Hamiltonian $\mathcal{H}$ can be obtained from the Fourier transform of the survival probability $\langle\psi \mid \psi(t)\rangle$ of a random pure state [33].

In fact, the relation (13) turns out to be useful for any arbitrary pure state $|\tilde{\psi}\rangle$ (which is not necessarily drawn at random). The local density of states $P(E)$ of $|\tilde{\psi}\rangle$, i. e., the spectral distribution of $|\tilde{\psi}\rangle$, is then defined as

$$P(E) = \sum_n |\langle n \mid \tilde{\psi}\rangle|^2\, \delta(E - E_n), \tag{14}$$

where $|n\rangle$ are the eigenvectors of $\mathcal{H}$ with corresponding eigenvalues E_n. Analogous to Eq. (13), $P(E)$ can be written as the Fourier transform of the survival probability of $|\tilde{\psi}\rangle$ [33, 70],

$$P(E) \propto \int_{-t_{\max}}^{+t_{\max}} e^{itE}\langle\tilde{\psi} \mid \tilde{\psi}(t)\rangle\mathrm{d}t. \tag{15}$$

Relying on the forward propagation of pure states discussed in Sec. 3.1, it is thus possible to access $\Omega(E)$ and $P(E)$. Note that Eqs. (13) and (15) only provide the overall shape (within the resolution ΔE) of $\Omega(E)$ and $P(E)$, while single eigenstates are difficult to resolve [71, 72].

As an example, let us consider the spin-1/2 XXZ chain,

$$\mathcal{H} = J\sum_{\ell=1}^{L}\left(S_\ell^x S_{\ell+1}^x + S_\ell^y S_{\ell+1}^y + \Delta S_\ell^z S_{\ell+1}^z\right), \tag{16}$$

where S_ℓ^i, $i \in \{x, y, z\}$ are the components of the corresponding spin-1/2 operators at the site ℓ, L is the number of lattice sites, $J = 1$ describes the antiferromagnetic coupling constant, and $\Delta > 0$ is the anisotropy in the

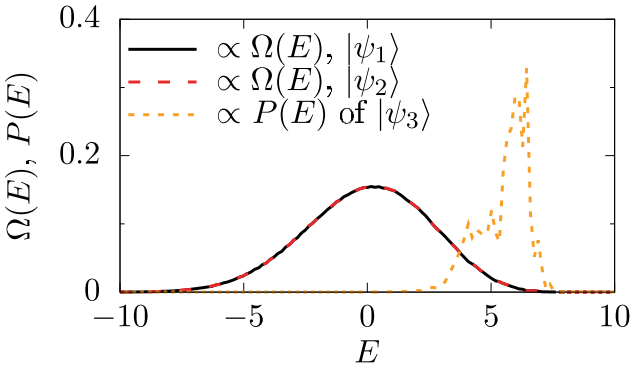

Figure 1: (Color online) Density of states $\Omega(E)$ of a spin-1/2 XXZ chain with $\Delta = 1.5$ and $L = 24$ sites, obtained from two independently drawn random states $|\psi_1\rangle$ and $|\psi_2\rangle$. The local density of states $P(E)$ is shown for a nonrandom state $|\psi_3\rangle$. Data is adapted from [71].

z-direction. In Figure 1, the density of states $\Omega(E)$ is shown for the XXZ chain (16) with $L = 24$ and $\Delta = 1.5$, obtained via Eq. (13) with two independently drawn random states $|\psi_1\rangle$ and $|\psi_2\rangle$. As can be seen in Figure 1, $\Omega(E)$ has a broad and Gaussian shape. Moreover, $\Omega(E)$ is essentially the same for the two random states, which confirms the accuracy of the typicality approach. In addition, we show $P(E)$ for a nonrandom state $|\psi_3\rangle$, which is sharply peaked at the borders of the spectrum [71].

3.3 Time-dependent equilibrium correlation functions

Let us now turn to quantum many-body dynamics within the framework of LRT. Within LRT, central quantities of interest are time-dependent correlation functions $C_{AB}(t)$ of two operators A and B evaluated in equilibrium,

$$C_{AB}(t) = \langle A(t)B\rangle_{\text{eq}} = \frac{\text{Tr}[A(t)Be^{-\beta\mathcal{H}}]}{Z}, \tag{17}$$

where Z is again the canonical partition function as defined in Eq. (3), and $A(t)$ is the time-evolved operator in the Heisenberg picture. Analogous to Eq. (4), $C_{AB}(t)$ can be rewritten according to [27–29],

$$\langle A(t)B\rangle_{\text{eq}} \approx \frac{\langle\psi_\beta(t)\,|\,A\,|\,\varphi_\beta(t)\rangle}{\langle\psi_\beta(0)\,|\,\psi_\beta(0)\rangle}, \tag{18}$$

where we have introduced two auxiliary pure states,

$$|\varphi_\beta(t)\rangle = e^{-i\mathcal{H}t}Be^{-\beta\mathcal{H}/2}|\psi\rangle, \tag{19}$$

$$|\psi_\beta(t)\rangle = e^{-i\mathcal{H}t}e^{-\beta\mathcal{H}/2}|\psi\rangle, \tag{20}$$

and $|\psi\rangle$ is a random state drawn from the full Hilbert space, cf. Eq. (5). Importantly, in contrast to Eq. (17), the time (and temperature) argument in Eq. (18) is now a property of the pure states and not of the operators anymore. According to, e. g., Eq. (8), $|\varphi_\beta(t)\rangle$ and $|\psi_\beta(t)\rangle$ can be evolved in real (and imaginary) time.

In the context of transport, an interesting quantity is the current autocorrelation function $C_{jj}(t)$, which is defined according to Eq. (17) with $A = B = j$, where j is the current operator. Note that the Fourier transform of $C_{jj}(t)$ is related to the conductivity via the Kubo formula [14, 73].

For concreteness, let us (again) consider the XXZ chain (16). In this case, the spin current operator j takes on the form [73],

$$j = J\sum_{\ell=1}^{L}(S_\ell^x S_{\ell+1}^y - S_\ell^y S_{\ell+1}^x). \tag{21}$$

In Refs. [29, 74], $C_{jj}(t)$ was studied by means of DQT for the XXZ chain with particular focus on infinite temperature $\beta = 0$. This infinite-temperature current autocorrelation function is exemplarily shown in Figure 2 for $\Delta = 1$ and $L = 33$. To demonstrate the smallness of the statistical error of DQT, we show results obtained from two independently drawn random states. As can be seen in Figure 2, both curves agree very well with each other for this choice of β and L, even in the semi-logarithmic plot used. (For further numerical data of $C_{jj}(t)$ see also Figure 8 below.)

In addition to the XXZ chain, DQT has been used to study $C_{jj}(t)$ for a variety of other low-dimensional systems, such as spin chains with next-nearest neighbor interactions [71] and with spin quantum number $S > 1/2$ [59], spin ladders [75–77] (also for energy currents), as well as Fermi-Hubbard chains [78]. The possibility to calculate $C_{jj}(t)$ by means of DQT for large systems and long time scales has proven to be very useful to extract transport

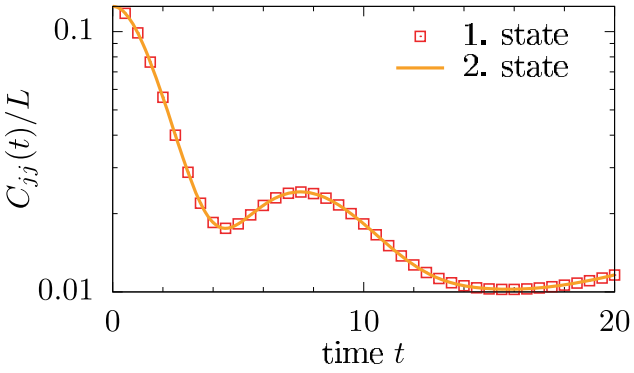

Figure 2: (Color online) Current autocorrelation function $C_{jj}(t)$ at $\beta = 0$ for the spin-1/2 XXZ chain with $\Delta = 1$, obtained by DQT for $L = 33$ sites. The calculation is done for two independently drawn states (from the symmetry subsector with momentum $k = 0$). Data is adapted from Ref. [74].

coefficients, including (the finite-size scaling of) dc conductivities, diffusion constants, and Drude weights, for integrable and nonintegrable models [29, 56, 59, 71, 74–78].

Another interesting quantity in the context of transport are the spatio-temporal correlation functions $C_{\ell,\ell'}(t)$ of, e. g., spin, which are defined according to Eq. (17) with $A = S^z_\ell$ and $B = S^z_{\ell'}$,

$$C_{\ell,\ell'}(t) = \langle S^z_\ell(t) S^z_{\ell'} \rangle_{\text{eq}}. \tag{22}$$

While a calculation of $C_{\ell,\ell'}(t)$ can be done according to Eq. (18), a simplification is possible at infinite temperature $\beta = 0$. Namely, at $\beta = 0$, one can introduce the pure state [77]

$$|\psi'(0)\rangle = \frac{\sqrt{S^z_{\ell'} + c}|\psi\rangle}{\sqrt{\langle\psi \mid \psi\rangle}}, \tag{23}$$

where $|\psi\rangle$ is again drawn randomly according to Eq. (5), and the constant c is chosen such that $S^z_{\ell'} + c$ has nonnegative eigenvalues. Using Eq. (23), one finds

$$C_{\ell,\ell'}(t) \approx \langle \psi'(t) \mid S^z_\ell \mid \psi'(t) \rangle. \tag{24}$$

Thus, it is possible to calculate $C_{\ell,\ell'}(t)$ just from one auxiliary state [59], in contrast to the current autocorrelations $C_{jj}(t)$, where two states have to be evolved in time, cf. Eqs. (19) and (20).

As an example, the equal-site spin-spin correlation function $C_{L/2,L/2}(t)$ at lattice site $\ell = L/2$ is shown in Figure 3 for spin-1/2 XXZ chains with two different lengths $L = 14$ and $L = 28$ [79]. (Note that due to periodic boundary conditions, the specific lattice site ℓ is arbitrary.) As a demonstration of the accuracy of the DQT approach, the calculation is done for two independently drawn pure states $|\psi\rangle$. While the DQT data closely follows the exact result at $L = 14$, the residual statistical fluctuations disappear almost completely for $L = 28$. Note that while we have chosen the XXZ chain to demonstrate the accuracy of DQT for $C_{jj}(t)$ [Figure 2] and for $C_{L/2,L/2}(t)$ [Figure 3], similar curves can be obtained for other models and observables as well. For additional comparisons between DQT data and exact ensemble averages, see, e. g., Refs. [29, 60].

As another example, the full time-space profile $C_{\ell,L/2}(t)$ is shown in Figure 4 for a spin-1/2 XXZ chain with next-nearest neighbor interactions and $L = 36$ sites [71]. While at $\beta = 0$ different lattice sites are uncorrelated at $t = 0$, correlations start to build up for $t > 0$.

A very similar example is shown in Figure 5, where the spatio-temporal correlations for spin and energy densities

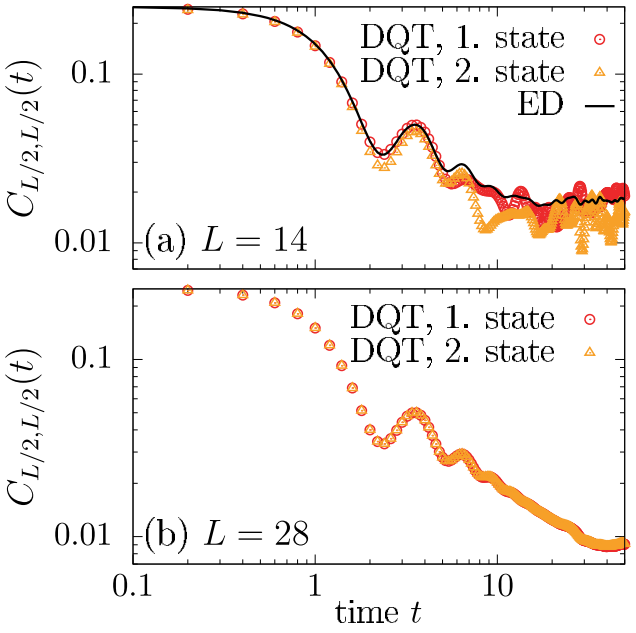

Figure 3: (Color online) Equal-site spin-spin correlation function $C_{L/2,L/2}(t)$ for spin-1/2 XXZ chains ($\Delta = 1$) with (a) $L = 14$ sites and (b) $L = 28$ sites. For $L = 14$, ED is compared to DQT for two different random pure states. While ED is unfeasible for $L = 28$, the statistical fluctuations of the typicality approximation become negligible for this system size. Data is adapted from Ref. [79].

are depicted at fixed times. Yet, the model is a spin-1/2 Heisenberg ladder,

$$\mathcal{H} = J_\parallel \sum_{l=1}^{L} \sum_{k=1}^{2} \boldsymbol{S}_{l,k} \cdot \boldsymbol{S}_{l+1,k} + J_\perp \sum_{l=1}^{L} \boldsymbol{S}_{l,1} \cdot \boldsymbol{S}_{l,2}, \tag{25}$$

where $J_\parallel$ ($J_\perp$) denotes the coupling on the legs (rungs). The data in Figure 5 are obtained for $J_\parallel = J_\perp = 1$ and $L = 20$, i. e., 40 lattice sites in total [77]. For all times shown in Figure 5, one finds that the profiles $C_{\ell,L/2}(t)$ are convincingly

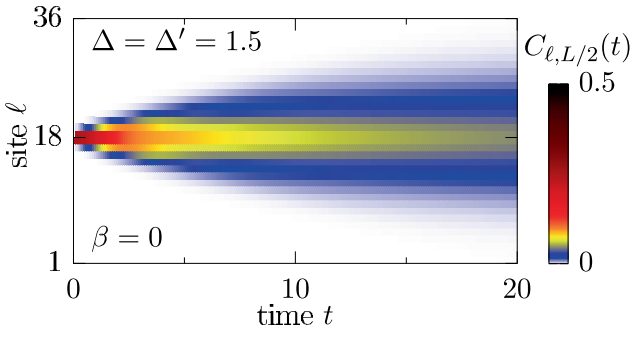

Figure 4: (Color online) Time-space plot of the infinite-temperature spin-spin correlation function $C_{\ell,L/2}(t) = \langle S^z_\ell(t) S^z_{L/2} \rangle_{\text{eq}}$ for a spin-1/2 XXZ chain of length $L = 36$, nearest neighbor ($\Delta = 1.5$) and next-nearest neighbor ($\Delta' = 1.5$) coupling. Data is adapted from Ref. [71].

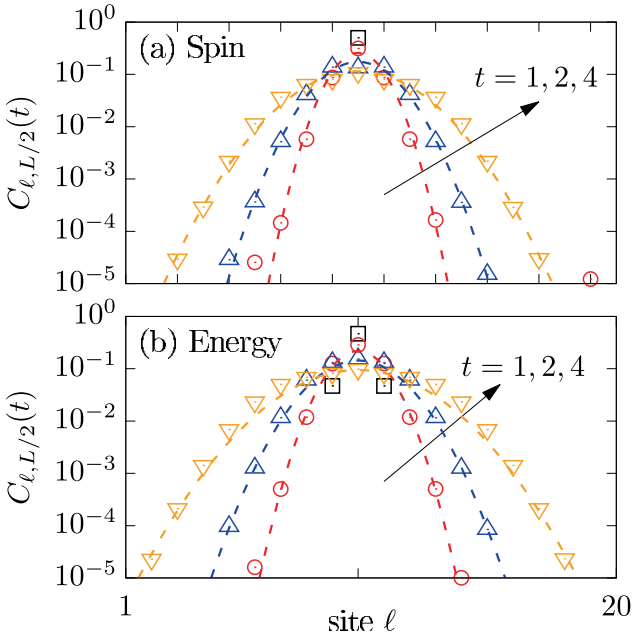

Figure 5: (Color online) Spin-spin correlation function $C_{\ell,L/2}(t)$ at fixed times, $t = 0$ (δ peak) and $t = 1, 2, 4$ (arrow), for a spin-1/2 Heisenberg ladder of length $L = 20$ (i. e., 40 lattice sites), at high temperatures $\beta = 0$. Dashed lines are Gaussian fits to the data. Panel (a) shows spin densities, while panel (b) shows local energies. Data is adapted from Ref. [77].

described by Gaussians, which illustrates once again the high accuracy of the DQT approach in the semi-logarithmic plot used. Such a Gaussian spreading has been interpreted as a clear signature of high-temperature spin and energy diffusion in this and other models [57, 59, 71, 80, 81].

In addition, DQT has been used to obtain spatio-temporal correlation functions $C_{\ell,\ell'}(t)$ in a number of other models. Remarkably, clean Gaussian profiles have been found in various parameter regimes, even for integrable models such as the spin-1/2 XXZ chain [57] or the one-dimensional Fermi-Hubbard model [80]. Other classes of models which have been studied in this way include the spin-1 XXZ chain [59] as well as spin models with quenched disorder [59, 82].

3.4 Applications to far-from-equilibrium dynamics

Nonequilibrium scenarios in isolated quantum systems can be induced via explicitly time-dependent Hamiltonians or, e. g., by means of quantum quenches [83]. For instance, the system can be initially in an eigenstate of some Hamiltonian $\mathcal{H}_1$ while the subsequent dynamics are governed by a different Hamiltonian $\mathcal{H}_2$.

Here, we discuss an alternative type of quench, where the system starts in a Gibbs state with respect to (w.r.t.) some initial Hamiltonian $\mathcal{H}_1$ (see Figure 6),

$$\rho(0) = \frac{e^{-\beta\mathcal{H}_1}}{Z}. \tag{26}$$

We then consider a quantum quench, where $\mathcal{H}_1$ is changed to some other Hamiltonian $\mathcal{H}_2$. The system then is in a nonequilibrium state and evolves unitarily according to the new Hamiltonian,

$$\rho(t) = e^{-i\mathcal{H}_2 t}\rho(0)e^{i\mathcal{H}_2 t}. \tag{27}$$

The post-quench Hamiltonian can, for instance, be created by adding or removing a static (weak or strong) force of strength ϵ to the initial Hamiltonian, i. e., $\mathcal{H}_2 = \mathcal{H}_1 \pm \epsilon A$, where the operator A is conjugated to the force [13, 58, 84, 85]. The resulting expectation value dynamics of, e. g., the operator A is given by

$$\langle A(t)\rangle = \mathrm{Tr}[\rho(t)A], \tag{28}$$

and its evaluation in principle requires complete diagonalization of both $\mathcal{H}_1$ and $\mathcal{H}_2$. As before, this

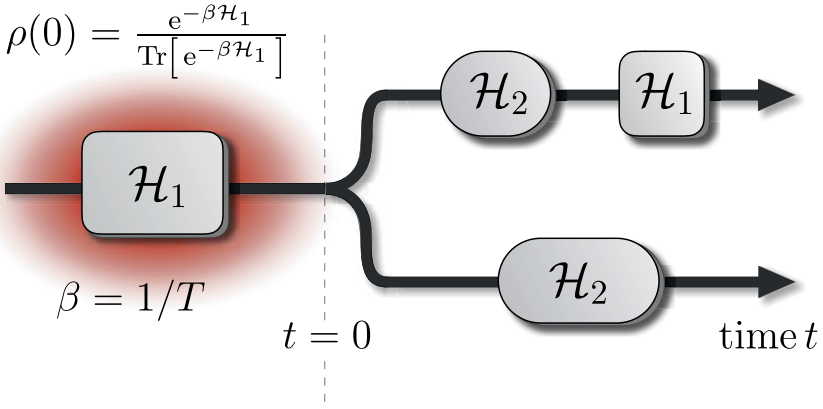

Figure 6: (Color online) Sketch of the quench protocol. The system starts in a Gibbs state with respect to some initial Hamiltonian $\mathcal{H}_1$. For times $t > 0$, the system evolves unitarily according to some other Hamiltonian $\mathcal{H}_2$ as per $\rho(t) = e^{-i\mathcal{H}_2 t}\rho(0)e^{i\mathcal{H}_2 t}$. This protocol can also be modified by switching back to the original Hamiltonian $\mathcal{H}_1$ (shown in the upper branch on the right hand side) or by further changes of the Hamiltonian in time.

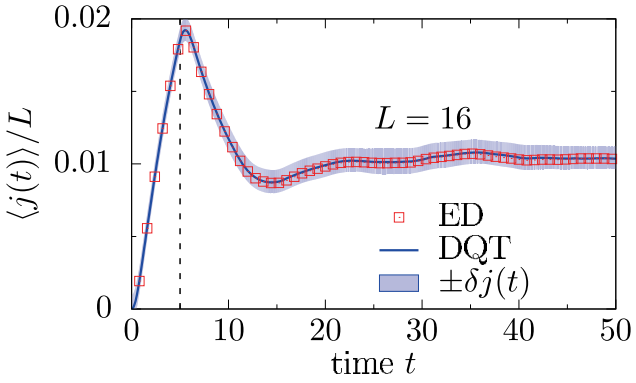

Figure 7: (Color online) Out-of-equilibrium dynamics of the spin current j in the spin-1/2 XXZ chain with $\Delta = 0.5$ and $L = 16$, starting from a thermal state with $\beta = 1$. For times $0 < t < 5$, an external force acts on the system, which gives rise to an additional term $\propto j$ within the Hamiltonian. Results from the typicality approach are compared to ED. DQT data are averaged over $N = 100$ random initial states and the shaded area indicates the standard deviation. Data is adapted from Ref. [44].

diagonalization can be circumvented by preparing a typical pure state [13, 43, 58, 84, 85],

$$|\Psi(0)\rangle = \frac{\mathrm{e}^{-\beta\mathcal{H}_1/2}|\psi\rangle}{\sqrt{\langle\psi\,|\,\mathrm{e}^{-\beta\mathcal{H}_1}|\psi\rangle}}, \tag{29}$$

which mimics the density matrix (26), and the reference state $|\psi\rangle$ is again randomly drawn from the full Hilbert space, cf. Eq. (5). Both the imaginary-time evolution w.r.t. $\mathcal{H}_1$ and the real-time evolution w.r.t. $\mathcal{H}_2$ can be done following Sec. 3.1. In this way, one gets

$$\langle A(t)\rangle \approx \langle\Psi(t)|A|\Psi(t)\rangle. \tag{30}$$

It is worth pointing out that the (simple) quench protocol above can be modified by additional changes of the Hamiltonian in time. A static force switched on at time $t = 0$ can, for instance, be removed again at some later time $t > 0$, see also Figure 6. Even for such protocols, the additional efforts of the DQT approach are minor compared to ED, where the diagonalization of multiple Hamiltonians has to be carried out.

In Figure 7, the nonequilibrium dynamics $\langle j(t)\rangle$ of the spin current is exemplarily depicted for a XXZ chain which is initially prepared in a thermal state at the finite temperature $\beta = 1$ (see caption of Figure 7 and Ref. [44] for a more detailed description of the protocol). Here, the accuracy of the DQT approach is demonstrated by comparing to data obtained by ED.

3.5 DQT and its extensions

In addition to the direct applications discussed above, DQT also is a useful tool to "boost" other (numerical or analytical) techniques, which can profit from accurate data for large system sizes. Two examples of such techniques, which have recently been combined with DQT, are numerical linked-cluster expansions (NLCE) and projection operator techniques.

3.5.1 NLCE

The key feature used in NLCE is the fact that the per-site value of an extensive quantity on an infinite lattice can be expanded in terms of its respective weights on all linked (sub-)clusters that can be embedded in the lattice. While NLCE is described in detail and generality in [86, 87], this section focuses on practical aspects of NLCE, particularly on its combination with DQT to calculate, e. g., current-current correlation functions of one-dimensional systems. The starting point of a corresponding NLCE is the expression

$$\frac{\langle j(t)j\rangle_{\mathrm{eq}}}{L} = \sum_c \mathcal{L}_c W_c(t), \tag{31}$$

where W_c is the weight of a cluster c with multiplicity $\mathcal{L}_c$. To avoid redundant computations, the multiplicity factor (divided by the total number of lattice sites) accounts for all clusters, which are symmetrically or topologically related to one representative cluster and therefore yield the same weight. The weight of each cluster is evaluated by the inclusion-exclusion principle

$$W_c(t) = \langle j(t)j\rangle_{\mathrm{eq}}^{(c)} - \sum_{s\subset c} W_s(t), \tag{32}$$

where the weights of all embedded clusters s are subtracted from $\langle j(t)j\rangle_{\mathrm{eq}}^{(c)}$ evaluated on the cluster c.

Since the maximum treatable cluster size is naturally limited by the available computational resources, the sum in Eq. (31) has to be truncated to a maximum size $c_{\max}$. In one dimension, this truncated sum reduces to the difference of the autocorrelation functions of the two largest open-boundary chains with length $c_{\max}$ and $c_{\max} - 1$, i. e.,

$$\sum_{c=2}^{c_{\max}} W_c(t) = \langle j(t)j\rangle_{\mathrm{eq}}^{(c_{\max})} - \langle j(t)j\rangle_{\mathrm{eq}}^{(c_{\max}-1)}. \tag{33}$$

As demonstrated in Ref. [88], this rather simple formula can have a better convergence towards the thermodynamic limit than a standard finite-size scaling at effectively equal computational cost.

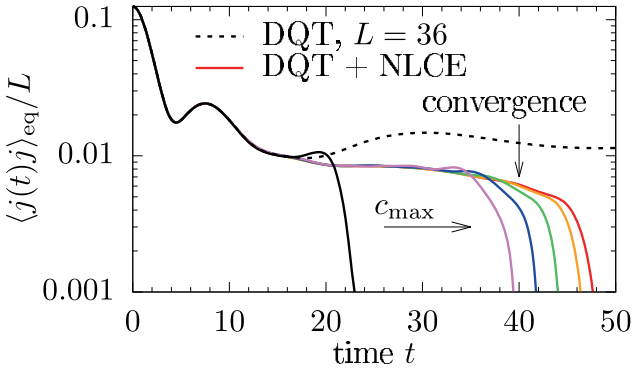

Figure 8: (Color online) Current-current correlation function $\langle j(t)j\rangle_{\rm eq}/L$ in the XXZ chain ($\Delta = 1$) at $\beta = 0$. Dashed line indicates data obtained by DQT for $L = 36$ and periodic boundary conditions. Solid lines are obtained by the combination of DQT and NLCE for expansion orders $c_{\rm max} = 18, 32, 34, 36, 38, 39$ (arrow). Data is adapted from Refs. [88, 92].

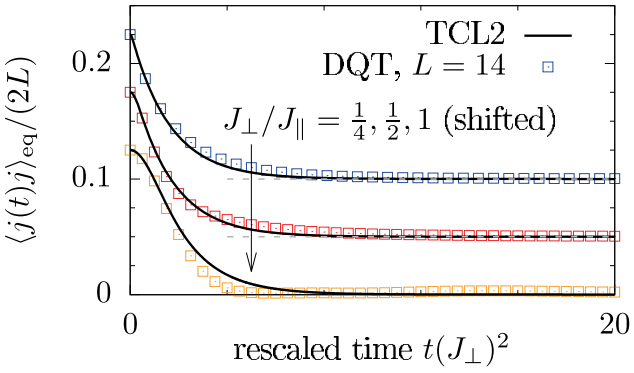

Figure 9: (Color online) Current-current correlation function for spin-1/2 XX ladders ($J_\parallel = 1$) with different interchain couplings $J_\perp$ (shifted for better visibility). Symbols denote exact data obtained by DQT for length $L = 14$, i. e., 28 spins in total. The solid lines indicate the prediction from the (second order) TCL projection operator method, cf. Eq. (35). Data is adapted from Ref. [92].

As shown in Figure 8, the current autocorrelation function for the spin-1/2 Heisenberg chain directly obtained by DQT for a large system with $L = 36$ still exhibits notable finite-size effects for times $t > 20$, whereas corresponding DQT + NLCE data is already converged for these times. Due to the truncation to a maximum cluster size $c_{\rm max}$, however, the expansion eventually breaks down and only yields reliable results up to a maximum time, which increases with $c_{\rm max}$ [88–90]. For the specific example in Figure 8, this maximum time is $t_{\rm max} \sim 40$ for the maximum cluster size $c_{\rm max} = 39$ calculated.

When studying thermodynamic quantities, for which the NLCE was originally introduced, using larger cluster sizes similarly improves the convergence of the expansion down to lower temperatures [87, 91]. Either way, it is thus desirable to access cluster sizes as large as possible and DQT can be used to evaluate the contributions of clusters beyond the range of ED. Since the difference in Eq. (33) could be sensitive to small statistical errors, it might be recommended to average the DQT results over multiple random pure states, in particular in higher dimensions, where the NLCE expression is not just a single difference.

3.5.2 Projection operator techniques

The DQT approach can also be used in the context of projection operator techniques, e. g., the so-called time-convolutionless (TCL) projection operator method. These techniques can be applied to situations where a closed quantum system with Hamiltonian $\mathcal{H}_0$ is perturbed by an operator $\mathcal{V}$ with strength λ, such that the total Hamiltonian takes on the form

$$\mathcal{H} = \mathcal{H}_0 + \lambda\mathcal{V}. \tag{34}$$

In this setting, one then chooses a suitable projection on the relevant degrees of freedom to obtain a systematic perturbation expansion for the reduced dynamics. We refer to [92–95] for a detailed description of the TCL method and do not discuss it here in full generality.

Choosing a simple projection onto A only and considering the specific initial conditions $\rho(0) \sim A$ yields in second order of the perturbation [92, 95]

$$\langle A(t)\rangle_{\mathcal{H}} = \langle A(t)\rangle_{\mathcal{H}_0} \exp\left[-\lambda^2 \int_0^t {\rm d}t'\, \gamma_2(t')\right], \tag{35}$$

where the second-order damping rate $\gamma_2(t)$ is given by

$$\gamma_2(t) = -\int_0^t \frac{{\rm Tr}\{[A, \mathcal{V}_{\rm I}(t')][A, \mathcal{V}]\}}{\langle A^2\rangle}{\rm d}t' \tag{36}$$

and the index I indicates operators in the interaction picture.

The calculation of Eq. (36) can be conveniently done using typical states and becomes especially simple in the case where the observable of interest is conserved under the unperturbed Hamiltonian, i. e., $[A, \mathcal{H}_0] = 0$. By defining $\mathcal{K} = [A, \mathcal{V}]$ and $\mathcal{K}_{\rm I}(t) = e^{i\mathcal{H}_0 t}\mathcal{K}e^{-i\mathcal{H}_0 t}$, the numerator of Eq. (36) can be calculated as

$${\rm Tr}[\mathcal{K}_{\rm I}(t)\mathcal{K}] \propto \langle\psi(t)|\mathcal{K}|\varphi(t)\rangle, \tag{37}$$

with the auxiliary states

$$|\psi(t)\rangle = \mathrm{e}^{-i\mathcal{H}_0 t}|\psi\rangle, \tag{38}$$

$$|\varphi(t)\rangle = \mathrm{e}^{-i\mathcal{H}_0 t}\mathcal{K}|\psi\rangle. \tag{39}$$

In [92], the quality of the second-order prediction (35) was numerically studied for the example of the current autocorrelation functions $\langle j(t)j\rangle_{\mathrm{eq}}$ in spin-1/2 ladder systems, where the interactions on the rungs of the ladder are treated as a perturbation to the otherwise uncoupled legs. As depicted in Figure 9, the second-order prediction agrees convincingly with exact data obtained by DQT for different strengths of the perturbation.

4 Conclusion

To summarize, we have discussed several applications of DQT and its usefulness as a numerical approach to the real-time dynamics of quantum many-body systems. The main idea of this typicality approach is to approximate ensemble expectation values via single pure states which are randomly drawn from a high-dimensional Hilbert space. In particular, time (temperature) dependencies of expectation values can be obtained by iteratively solving the Schrödinger equation in real (imaginary) time, e. g., by means of Runge-Kutta schemes or more sophisticated methods.

First, we have described that DQT can be used to study the (local) density of states as well as equilibrium correlation functions for long time scales and comparatively large system sizes beyond the range of standard ED. Especially in the context of transport, the calculation of current autocorrelations and density-density correlations by means of DQT is possible. Furthermore, we have outlined that DQT is suitable to investigate also the far-from-equilibrium dynamics resulting from certain quench protocols. For instance, an initial Gibbs state is properly imitated by a typical pure state and nonequilibrium conditions are induced by removing or adding an external force. Eventually, we have discussed that DQT can additionally be combined with other approaches. As one example, we have shown that the convergence of NLCE can be improved by evaluating the contributions of larger clusters by means of DQT. As another example, we have discussed that DQT allows to compute memory kernels which arise in projection operator methods such as the TCL technique.

While this paper has illustrated the usefulness of DQT for selected applications in the context of transport and thermalization, we should stress that there certainly are other applications of DQT which have not been mentioned by us. One such application, as done in, e. g., [96], is the spreading of quantum information measured by so-called out-of-time-ordered correlators (OTOCs) of the form [97],

$$C(t) = \frac{\mathrm{Tr}[A(t)BA(t)B]}{d}, \tag{40}$$

where the operators A and B are, for instance, local magnetization densities S^z_ℓ at two different lattice sites. Similar to the correlation functions discussed in Eq. (17), the OTOC in Eq. (40) can be approximated as the overlap $C(t) \approx \langle\psi_2(t)\,|\,\psi_1(t)\rangle$ of the two auxiliary states $|\psi_1(t)\rangle = A(t)B|\psi\rangle$ and $|\psi_2(t)\rangle = BA(t)|\psi\rangle$, where $|\psi\rangle$ is again a Haar-random state [96].

In conclusion, the concept of DQT offers a rather simple yet remarkably useful approach to study the real-time dynamics of quantum many-body systems. It is our hope that the examples discussed in this paper motivate its application in other areas as well.

Acknowledgments: This work has been funded by the Deutsche Forschungsgemeinschaft (DFG) – Grants No. 397067869 (STE 2243/3-1), No. 355031190 – within the DFG Research Unit FOR 2692.

References

[1] I. Bloch, J. Dalibard, and S. Nascimbène, *Nat. Phys.*, vol. 8, p. 267, 2012.
[2] R. Blatt and C. F. Roos, *Nat. Phys.*, vol. 8, p. 277, 2012.
[3] A. Polkovnikov, K. Sengupta, A. Silva, and M. Vengalattore, *Rev. Mod. Phys.*, vol. 83, p. 863, 2011.
[4] J. Eisert, M. Friesdorf, and C. Gogolin, *Nat. Phys.*, vol. 11, p. 124, 2015.
[5] L. D'Alessio, Y. Kafri, A. Polkovnikov, and M. Rigol, *Adv. Phys.*, vol. 65, p. 239, 2016.
[6] C. Gogolin and J. Eisert, *Rep. Prog. Phys.*, vol. 79, p. 056001, 2016.
[7] F. Borgonovi, F. Izrailev, L. Santos, and V. Zelevinsky, *Phys. Rep.*, vol. 626, p. 1, 2016.
[8] M. Buchanan, *Nat. Phys.*, vol. 1, p. 71, 2005.
[9] V. Khemani, A. Vishwanath, and D. A. Huse, *Phys. Rev. X*, vol. 8, p. 031057, 2018.
[10] B. Bertini, F. Heidrich-Meisner, C. Karrasch, T. Prosen, R. Steinigeweg, and M. Žnidarič, arXiv:2003.03334.
[11] M. Prüfer, P. Kunkel, H. Strobel, et al., *Nature*, vol. 563, p. 217, 2018.
[12] S. Erne, R. Bücker, T. Gasenzer, J. Berges, and J. Schmiedmayer, *Nature*, vol. 563, p. 225, 2018.
[13] J. Richter and R. Steinigeweg, *Phys. Rev. E*, vol. 99, p. 012114, 2019.

[14] R. Kubo, M. Toda, and N. Hashitsume, Statistical Physics II, 2nd ed., *Springer Series in Solid-State Sciences*, Vol. 31, Berlin, Heidelberg, Springer, p. 279, 1991.
[15] U. Schollwöck, *Ann. Phys. (N. Y).*, vol. 326, p. 96, 2011.
[16] S. Paeckel, T. Köhler, A. Swoboda, S. R. Manmana, U. Schollwöck, and C. Hubig, *Ann. Phys. (N. Y).*, vol. 411, p. 167998, 2019.
[17] C. Bartsch and J. Gemmer, *Phys. Rev. Lett.*, vol. 102, p. 167998, 2009.
[18] P. Reimann, *Phys. Rev. E*, 97, p. 062129, 2018.
[19] R. Alben, M. Blume, H. Krakauer, and L. Schwartz, *Phys. Rev. B*, vol. 12, p. 4090, 1975.
[20] S. Lloyd, *Pure state quantum statistical mechanics and black holes, Phd thesis*, The Rockefeller University, 1988, arXiv: 1307.0378.
[21] H. De Raedt and P. de Vries, *Z. Phys. B*, vol. 77, p. 243, 1989.
[22] J. Jaklič and P. Prelovšek, *Phys. Rev. B*, vol. 49, p. 5065, 1994.
[23] J. Gemmer, M. Michel, and G. Mahler, *Quantum Thermodynamics*, Lecture Notes in Physics, Vol. 657, Springer, Berlin, Heidelberg, 2004.
[24] S. Popescu, A. J. Short, and A. Winter, *Nat. Phys.*, vol. 2, p. 754, 2006.
[25] S. Goldstein, J. L. Lebowitz, R. Tumulka, and N. Zanghì, *Phys. Rev. Lett.*, vol. 96, p. 050403, 2006.
[26] P. Reimann, *Phys. Rev. Lett.*, vol. 99, p. 160404, 2007.
[27] T. Iitaka and T. Ebisuzaki, *Phys. Rev. Lett.*, vol. 90, p. 047203, 2003.
[28] T. A. Elsayed and B. V. Fine, *Phys. Rev. Lett.*, vol. 110, p. 070404, 2013.
[29] R. Steinigeweg, J. Gemmer, and W. Brenig, *Phys. Rev. Lett.*, vol. 112, p. 120601, 2014.
[30] S. Okamoto, G. Alvarez, E. Dagotto, and T. Tohyama, *Phys. Rev. E*, vol. 97, p. 043308, 2018.
[31] Y. Yamaji, T. Suzuki, and M. Kawamura, arXiv:1802.02854.
[32] I. Rousochatzakis, S. Kourtis, J. Knolle, R. Moessner, and N. B. Perkins, *Phys. Rev. B*, vol. 100, p. 045117, 2019.
[33] A. Hams and H. De Raedt, *Phys. Rev. E*, vol. 62, p. 4365, 2000.
[34] P. de Vries and H. De Raedt, *Phys. Rev. B*, vol. 47, p. 7929, 1993.
[35] S. Sugiura and A. Shimizu, *Phys. Rev. Lett.*, vol. 108, p. 240401, 2012.
[36] S. Sugiura and A. Shimizu, *Phys. Rev. Lett.*, vol. 111, p. 010401, 2013.
[37] A. Wietek, P. Corboz, S. Wessel, B. Normand, F. Mila, and A. Honecker, *Phys. Rev. Research*, vol. 1, p. 033038, 2019.
[38] T. Iitaka and T. Ebisuzaki, *Phys. Rev. E*, vol. 69, p. 057701, 2004.
[39] D. N. Page, *Phys. Rev. Lett.*, vol. 71, p. 1291, 1993.
[40] L. Vidmar and M. Rigol, *Phys. Rev. Lett.*, vol. 119, p. 220603, 2017.
[41] J. Schnack, J. Richter, and R. Steinigeweg, *Phys. Rev. Research*, vol. 2, p. 013186, 2020.
[42] T. Monnai and A. Sugita, *J. Phys. Soc. Jpn.*, vol. 83, p. 094001, 2014.
[43] H. Endo, C. Hotta, and A. Shimizu, *Phys. Rev. Lett.*, vol. 121, p. 220601, 2018.
[44] J. Richter, M. H. Lamann, C. Bartsch, R. Steinigeweg, and J. Gemmer, Phys. Rev. E, vol. 100, p. 032124, 2019.
[45] J. M. Deutsch, *Phys. Rev. A*, vol. 43, p. 2046, 1991.
[46] M. Srednicki, *Phys. Rev. E*, vol. 50, p. 888, 1994.
[47] M. Rigol, V. Dunjko, and M. Olshanii, *Nature*, vol. 452, p. 854, 2008.
[48] L. F. Santos and M. Rigol, *Phys. Rev. E*, vol. 82, p. 031130, 2010.
[49] R. Steinigeweg, J. Herbrych, and P. Prelovšek, *Phys. Rev. E*, vol. 87, p. 012118, 2013.
[50] W. Beugeling, R. Moessner, and M. Haque, *Phys. Rev. E*, vol. 89, p. 042112, 2014.
[51] H. Kim, T. N. Ikeda, and D. A. Huse, *Phys. Rev. E*, vol. 90, p. 052105, 2014.
[52] R. Nandkishore and D. A. Huse, *Annu. Rev. Condens. Matter Phys.*, vol. 6, p. 15, 2015.
[53] R. Mondaini and M. Rigol, *Phys. Rev. E*, vol. 96, p. 012157, 2017.
[54] D. Jansen, J. Stolpp, L. Vidmar, and F. Heidrich-Meisner, *Phys. Rev. B*, vol. 99, p. 155130, 2019.
[55] I. M. Khaymovich, M. Haque, and P. A. McClarty, *Phys. Rev. Lett.*, vol. 122, p. 070601, 2019.
[56] R. Steinigeweg, J. Herbrych, F. Pollmann, and W. Brenig, *Phys. Rev. B*, vol. 94, p. 180401, 2016.
[57] R. Steinigeweg, F. Jin, D. Schmidtke, H. De Raedt, K. Michielsen, and J. Gemmer, *Phys. Rev. B*, vol. 95, p. 035155, 2017.
[58] J. Richter, J. Herbrych, and R. Steinigeweg, *Phys. Rev. B*, vol. 98, p. 134302, 2018.
[59] J. Richter, N. Casper, W. Brenig, and R. Steinigeweg, *Phys. Rev. B*, vol. 100, p. 144423, 2019.
[60] R. Steinigeweg, A. Khodja, H. Niemeyer, C. Gogolin, and J. Gemmer, *Phys. Rev. Lett.*, vol. 112, p. 130403, 2014.
[61] T. Heitmann and J. Schnack, *Phys. Rev. B*, vol. 99, p. 134405, 2019.
[62] L. P. Hughston, R. Jozsa, and W. K. Wootters, *Phys. Lett. A*, vol. 183, p. 14, 1993.
[63] H. De Raedt and K. Michielsen, *Host Publ.*, 2006.
[64] A. Nauts and R. E. Wyatt, *Phys. Rev. Lett.*, vol. 51, p. 2238, 1983.
[65] H. Tal-Ezer and R. Kosloff, *J. Chem. Phys.*, vol. 81, p. 3967, 1984.
[66] R. Kosloff, *Annu. Rev. Phys. Chem.*, vol. 45, p. 145, 1994.
[67] V. V. Dobrovitski and H. De Raedt, *Phys. Rev. E*, vol. 67, p. 056702, 2003.
[68] A. Weiße, G. Wellein, A. Alvermann, and H. Fehske, *Rev. Mod. Phys.*, vol. 78, p. 275, 2006.
[69] R. Kosloff, *J. Chem. Phys.*, vol. 150, p. 204105, 2019.
[70] M. Schiulaz, E. J. Torres-Herrera, and L. F. Santos, *Phys. Rev. B*, vol. 99, p. 174313, 2019.
[71] J. Richter, F. Jin, H. De Raedt, K. Michielsen, J. Gemmer, and R. Steinigeweg, *Phys. Rev. B*, vol. 97, p. 174430, 2018.
[72] D. M. Kennes, C. Karrasch, and A. J. Millis, *Phys. Rev. B*, vol. 101, p. 081106, 2020.
[73] F. Heidrich-Meisner, A. Honecker, and W. Brenig, *Eur. Phys. J. Spec. Top.*, vol. 151, p. 135, 2007.
[74] R. Steinigeweg, J. Gemmer, and W. Brenig, *Phys. Rev. B*, vol. 91, p. 104404, 2015.
[75] R. Steinigeweg, F. Heidrich-Meisner, J. Gemmer, K. Michielsen, and H. De Raedt, *Phys. Rev. B*, vol. 90, p. 094417, 2014.
[76] R. Steinigeweg, J. Herbrych, X. Zotos, and W. Brenig, *Phys. Rev. Lett.*, vol. 116, p. 017202, 2016.
[77] J. Richter, F. Jin, L. Knipschild, et al., *Phys. Rev. B*, vol. 99, p. 144422, 2019.
[78] F. Jin, R. Steinigeweg, F. Heidrich-Meisner, K. Michielsen, and H. De Raedt, *Phys. Rev. B*, vol. 92, p. 205103, 2015.
[79] B. N. Balz, J. Richter, J. Gemmer, R. Steinigeweg, and P. Reimann, in *Thermodynamics in the Quantum Regime*, Springer, Cham, pp. 413–433, 2018.
[80] R. Steinigeweg, F. Jin, H. De Raedt, K. Michielsen, and J. Gemmer, *Phys. Rev. E*, vol. 96, p. 020105, 2017.
[81] M. Ljubotina, M. Žnidarič, and T. Prosen, *Nat. Commun.*, vol. 8, p. 16117, 2017.

[82] J. Richter, D. Schubert, and R. Steinigeweg, *Phys. Rev. Research*, vol. 2, p. 013130, 2020.
[83] A. Mitra, *Annu. Rev. Condens. Matter Phys.*, vol. 9, p. 245, 2018.
[84] C. Bartsch and J. Gemmer, *EPL (Europhys. Lett.)*, vol. 118, p. 10006, 2017.
[85] J. Richter, J. Gemmer, and R. Steinigeweg, *Phys. Rev. E*, vol. 99, p. 050104, 2019.
[86] M. Rigol, T. Bryant, and R. R. P. Singh, *Phys. Rev. Lett.*, vol. 97, p. 187202, 2006.
[87] B. Tang, E. Khatami, and M. Rigol, *Comput. Phys. Commun.*, vol. 184, p. 557, 2013.
[88] J. Richter and R. Steinigeweg, *Phys. Rev. B*, vol. 99, p. 094419, 2019.
[89] I. G. White, B. Sundar, and K. R. A. Hazzard, arXiv:1710.07696.
[90] K. Mallayya and M. Rigol, *Phys. Rev. Lett.*, vol. 120, p. 070603, 2018.
[91] K. Bhattaram and E. Khatami, *Phys. Rev. E*, vol. 100, p. 013305, 2019.
[92] J. Richter, F. Jin, L. Knipschild, et al., arXiv:1906.09268.
[93] S. Chaturvedi and F. Shibata, *Z. Phys. B*, vol. 35, p. 297, 1979.
[94] H.-P. Breuer and F. Petruccione, *The Theory of Open Quantum Systems*, Oxford University Press, 2007.
[95] R. Steinigeweg, *Phys. Rev. E*, vol. 84, p. 011136, 2011.
[96] D. J. Luitz and Y. Bar Lev, *Phys. Rev. B*, vol. 96, p. 020406, 2017.
[97] J. Maldacena, S. H. Shenker, and D. Stanford, *J. High Energ. Phys.*, vol. 2016, p. 106, 2016.